

EFFECT OF CRACK ARRESTER FOR FOAM CORE SANDWICH PANEL UNDER MODE I, MODE II AND MIXED-MODE CONDITION

Hirokazu Matsuda*, Go Matsubara*, Yasuo Hirose*, Masaki Hojo**
 *Kawasaki Heavy Industries Ltd., **Kyoto University

Keywords: *Foam core, Sandwich structure, Crack arrester, Delamination suppression, Fracture mechanics, Energy release rate*

Abstract

Crack arresters were installed to suppress interfacial crack propagation between the facing and core of CFRP/foam core sandwich panels. The crack arrester effect was investigated using analytical and experimental methods. The energy release rate was calculated and evaluated by FE analyses. A considerable reduction in the energy release rate at the crack tip was observed as the tip approached the crack arrester. Fracture toughness test was carried out using sandwich panel specimens with the crack arrester under mode I type, mixed-mode type, and mode II type loadings. The effect of the crack arrester depends on loading type. This effect was enhanced with increasing contribution of mode II type component.

1 Introduction

Semi-monocoque constructions or skin/stringer configurations are widely adopted as the primary structure of civil aircraft made of metallic materials. When only metallic materials are replaced with carbon-fiber-reinforced-plastic (CFRP) using the conventional metallic structural concept, limitations in cost and weight saving among others arise, and the advantages of CFRP are not effectively exploited. A foam-core sandwich panel has a promising structural concept for the integral structure to exploit the advantages of CFRP such as cost, weight saving, and parts-count reduction [1-3]. However, structural integrity is lost as a result of interfacial cracks or the delamination between the surface skin and the core under static or fatigue loading. Thus, the development of a novel structural element for suppressing the extension of delamination caused by damage is one of the main issues in the application of the

foam-core sandwich panel in actual aircraft structures.

Hirose et al. proposed a new concept, i.e., the use of crack arresters, to suppress delamination (crack) propagating between the surface skin and the foam core of a sandwich panel [4-7]. They estimated the effect of the crack arrester using numerical simulation under mode I and mode II type loadings [4-7]. No such effect was confirmed under mixed-mode type loading.

In this study, we carried out a numerical evaluation of the arrester effect under mixed-mode type loading as well as under mode I and mode II type loadings [6, 7]. The arrester effect was also investigated experimentally by fracture toughness test under mode I type [6], mixed-mode type, and the mode II type [7] loadings. The influence of loading type was discussed from the viewpoint of stress distribution near the crack tip.

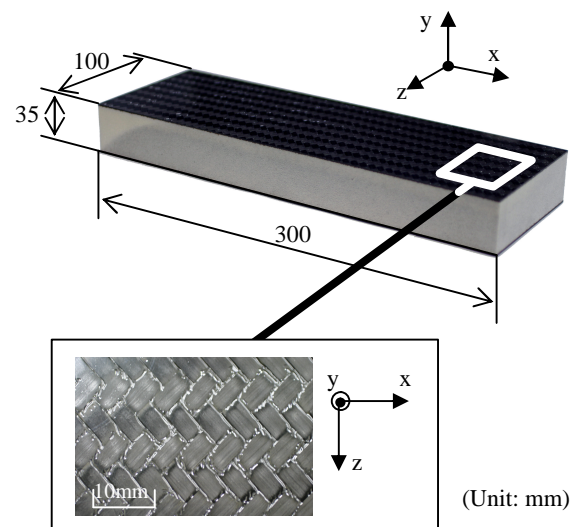


Fig.1 Specimen configuration

2 Foam core sandwich panel

2.1 Material and panel structure

The foam core sandwich panel specimens used were made of two materials: CFRP (Toho Tenax UT500/#135, graphite/epoxy twill weave fabric prepreg), and PMI (polymethacrylimide) foam core. The PMI foam core was placed between CFRP surface skins. The ply-orientations of the CFRP surface skin were $[(+45,-45)/(0,90)/(0,90)/(+45,-45)]_s$ with a nominal thickness of 3.2 mm. The surface skins and core were cocured without adhesive. An overview of the specimen is shown in Fig.1. The mechanical properties of the surface skin and PMI core are summarized in Table 1.

2.2 Microscopic structure of surface skin/core interface after fracture

Fig.2 shows a macroscopic photograph of the surface skin and the core of the specimen after the fracture toughness test. The resin was squeezed from the surface skin and impregnated into cells of the foam core adjacent to the skin. The thickness of the resin layer was about 0.34 mm, which is equivalent to the cell size. The photograph indicates that an interfacial crack propagates between this resin-impregnated layer and the original foam core.

2.3 New concept of crack arrester for foam core sandwich panel

Because an interfacial crack propagates between the resin layer and the foam core, a dissimilar material with higher stiffness, installed on the crack propagation path, is expected to suppress crack propagation. The concept of the crack arrester is shown in Fig.3. The semicylindrical shape crack arrester was placed between the CFRP surface skin and the foam core. The shape was selected considering production efficiency. Here, the straight portion of the arrester was attached to the surface skin.

The material of the crack arrester should have a higher modulus than the foam core material. One of the candidate materials for the arrester materials is CFRP (Toho Tenax UT500/#135). The fiber direction is perpendicular to the crack propagation direction in the case of CFRP. If the crack arrester decreases the energy release rate at crack tip below the fracture toughness of the skin-core interface under the same loading condition, the crack will be suppressed or stopped. This crack suppression effect of the arrester is estimated analytically in the following sections.

Table 1 Material properties of foam core sandwich panel

Material property	Resin	PMI Core
E (GPa)	4.1	1.67×10^{-1}
ν	0.330	0.180
G(GPa)	1.54	7.1×10^{-2}

Material property	CFRP (+45,-45)	CFRP (0,90)	CFRP (90)
E ₁₁ (GPa)	12.6	54.9	8.61
E ₂₂ (GPa)	8.61	8.61	8.61
E ₃₃ (GPa)	12.6	54.9	127
ν_{12}	0.330	0.330	0.550
ν_{23}	0.230	5.20×10^{-2}	2.20×10^{-2}
ν_{31}	0.780	0.051	0.330
G ₁₂ (GPa)	3.31	3.77	2.78
G ₂₃ (GPa)	3.31	3.77	4.23
G ₃₁ (GPa)	26.1	3.53	4.23

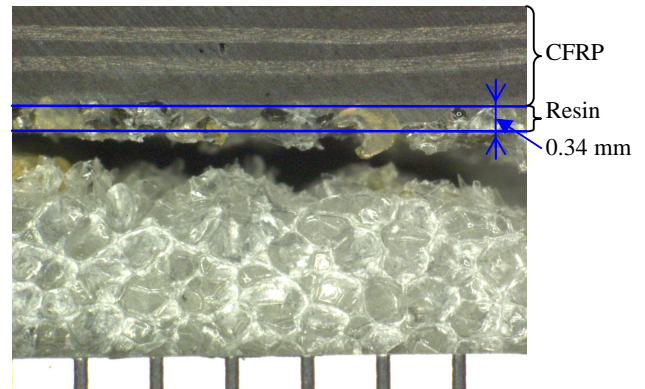


Fig.2 Optical micrograph of area around interface between skin and core

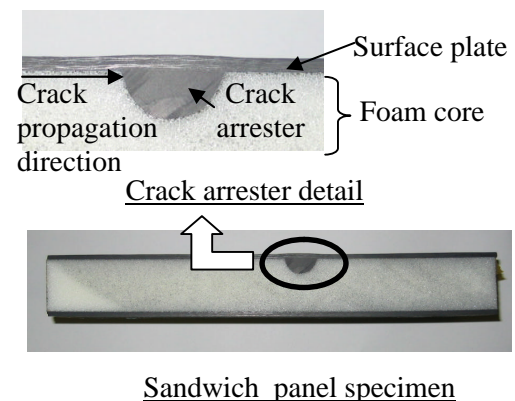


Fig.3 Crack arrester concept

3 Analysis of energy release rate

3.1 Model and boundary condition

The energy release rate G_A was calculated for different crack tip locations from the leading edge of the arrester to confirm the effect of the crack arrester. The G value for the specimen without the crack arrester, G_0 , was also calculated. Fig.4 shows the analytical models for mode I type (double cantilever beam (DCB)) [6], mixed-mode type (mixed mode bending (MMB)), and mode II type (ENF, end notched flexure (ENF)) [7] loadings. The shear loading component increases with decreasing length C of the arm for the MMB loading. Two cases, $C=50\text{mm}$ and $C=20\text{mm}$, for mixed-mode type loading were analyzed.

The commercial finite element code ABAQUS Ver.6.4.1 was used in this study. A two-dimensional small deformation elastic analysis was performed under plain strain condition to investigate the effect of the crack arrester. To evaluate the results of the fracture toughness test, a large deformation analysis was carried out. A typical mesh pattern of the crack

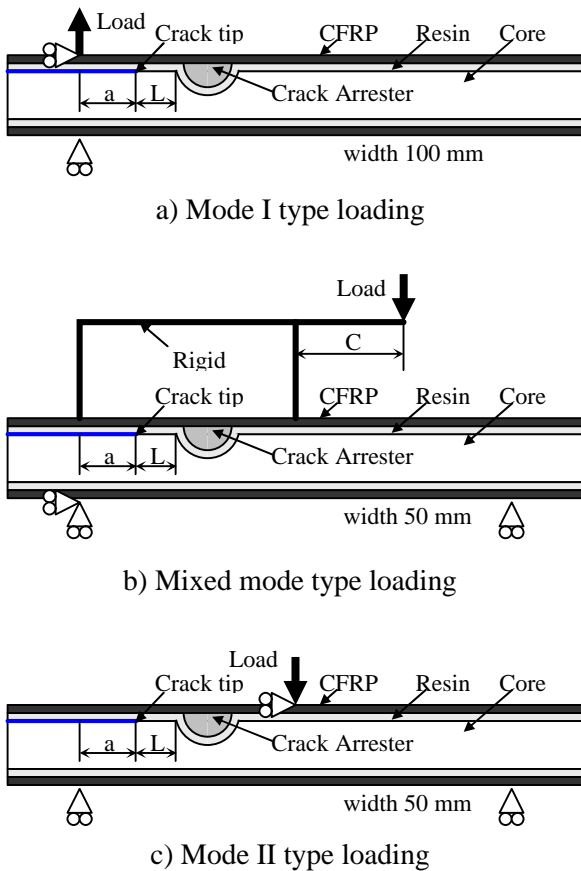


Fig.4 FE model of test specimen for fracture toughness test

arrester model is shown in Fig.5. Eight node isoparametric elements were used in this model. The element size at the crack tip was $4.25 \times 10^{-2} \text{ mm}$. G values were calculated using the modified crack closure integral (MCCI) method [7]. The G values were total energy release rates and consisted of the opening and shear components.

3.2 Analytical results

Fig.6 shows the analytical results of the G values with the crack arrester. L is the distance between the crack tip and the arrester edge. Here, the G values for the arrester specimen, $G_A(P,a)$, are normalized by those of the arrester-free specimen at the same crack length and the same applied load, $G_0(P,a)$. G values significantly decrease with decreasing L under any loading mode. Under mode II type loading, G starts to decrease before the crack tip reaches 20mm from the crack arrester edge. The influence of loading type is small. The rate of the G value decrease is slightly larger when the proportion of the shear loading component is higher.

Fig.7 shows the relationship between critical load and crack length. Critical load was estimated on

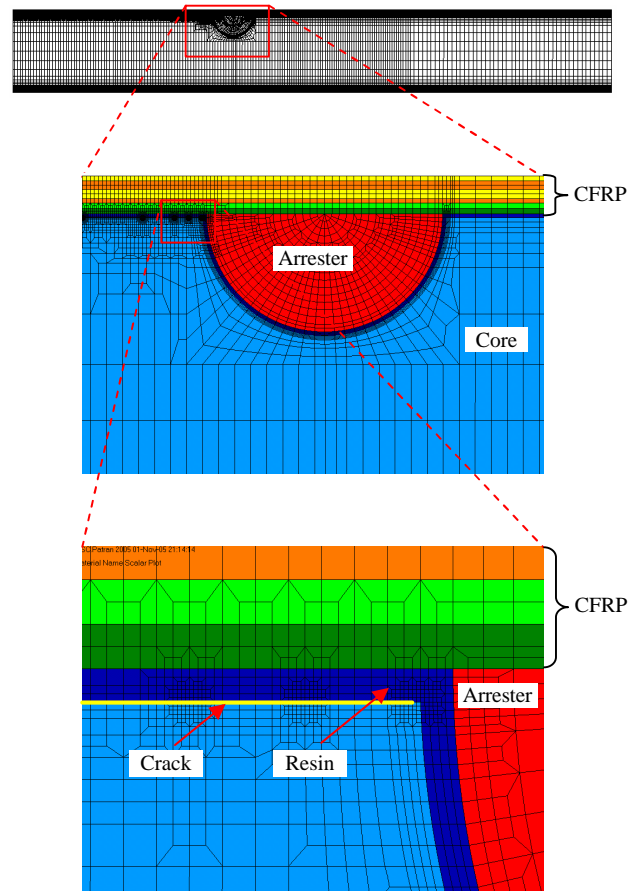


Fig.5 Typical FE mesh near crack arrester

the assumption that the net fracture toughness is constant for any loading type. Here, the critical load for the arrester specimen, P_A , is normalized by that of the arrester-free specimen having the same crack length, P_0 . The critical load P_A increases significantly with decreasing L regardless loading type. The P_C for mode II type loading is the highest; and it decreases with increasing fraction of mode I type component.

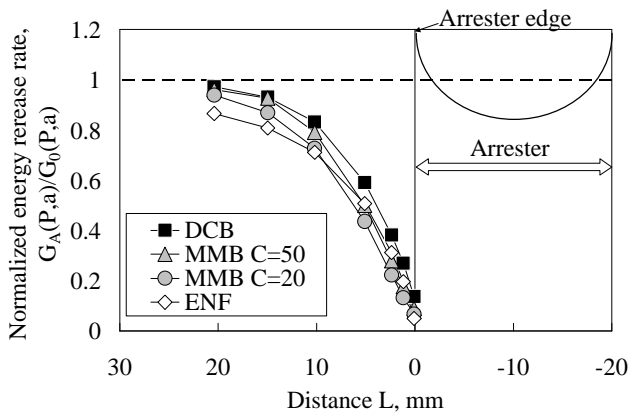


Fig.6 Relationship between normalized energy release rate G and distance L

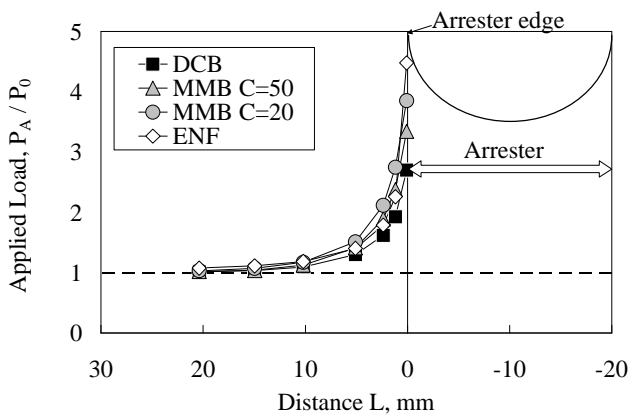


Fig.7 Relationship between normalized applied load P and distance L



Fig.8 Specimen and loading device for mixed-mode type loading test

4 Fracture toughness test

4.1 Specimen

The width of the specimen for mode I type loading is 100 mm, and those for mode II and mixed-mode type loadings are 50mm. The length of the specimens is 300 mm. An initial crack was introduced into the specimens by inserting polyimide films of 12.5 μm thickness and 100 mm length between the surface skin and the core during molding. The edge of the arrester was 20 mm from the edge of the film.

4.2 Experimental procedure

Fracture toughness test was carried out for mode I type [6], mixed-mode type and mode II type [7] loadings using a servo-hydraulic testing machine (Instron 8800, maximum capacity 5 kN; Instron 8501, maximum capacity 100 kN). The testing environment was at room temperature. The crosshead speed was 2 mm/min. The specimen was loaded until a crack extended up to a length less than 7 mm; the specimen was then unloaded. This procedure was repeated until the crack propagated up to the edge of arrester. Crack length was measured on both sides of the specimen using traveling optical microscopes at 200x magnification. Fig.8 shows the specimen and loading device for the fracture toughness test in mixed-mode type loading.

4.3 Experimental result

For the arrester-free specimen, the crack propagated straight at the interface between the resin and the core. For the arrester specimen, the crack also propagated straight at the interface under mode I and mixed-mode type loadings. On the other hand, the crack propagated at the interface between the resin and the core up to a point 1.5 mm from the edge of the arrester under mode II type loading. After the crack was arrested near the edge of the arrester, the specimen was unloaded and reloaded. Then, the crack kinked into the core.

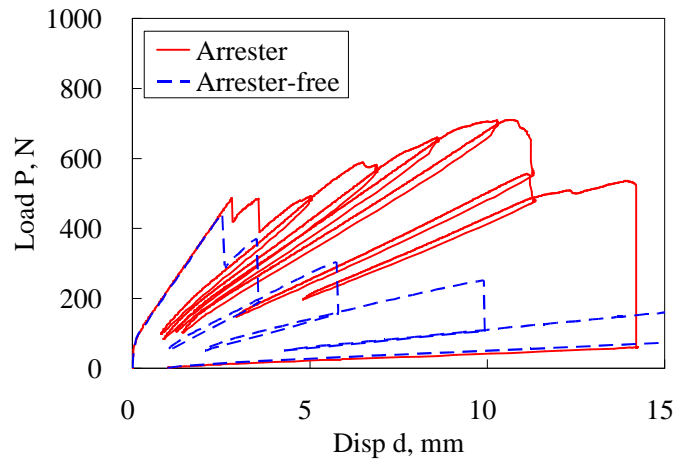
Fig.9 shows examples of load-displacement curves for the mode I type [6], the mixed-mode type and the mode II type [7] loadings. The blue lines indicate the results of the arrester-free specimens and the red ones indicate those of the arrester specimens. For the arrester-free specimens, the interfacial crack propagated unstably in a stick-slip manner under mode I and mixed-mode type loadings, while the crack propagated mechanically unstably under mode II type loading. For the crack arrester specimens, stable crack propagations were observed un-

der mode I and mixed-mode type loadings with increasing critical load as the crack propagated to the edge of the arrester. On the other hand, the crack propagated mechanically unstably and arrested near the edge of the arrester under mode II type loading. The load at the kinked point was similar to the first critical load.

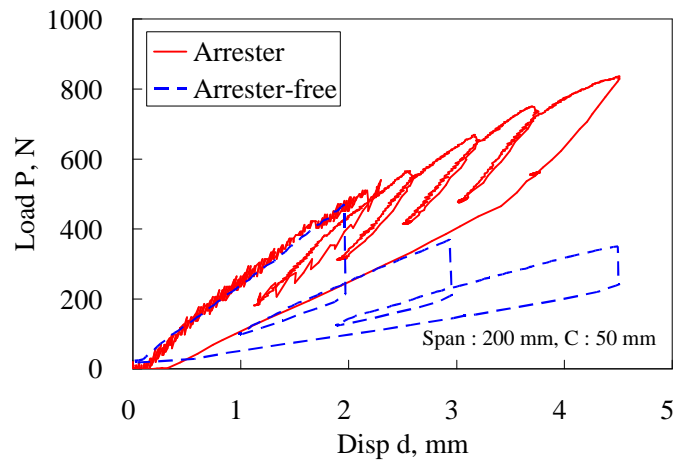
Fig.10 shows the relationship between fracture toughness, G_C , and crack length under mode I type [6], mixed-mode type, and mode II type [7] loadings in the fracture toughness test. Here, the crack arrester effects are described by apparent values, $G_C(\text{apparent})$. These apparent values, $G_C(\text{apparent}) = G_0(P_C, a)$, were obtained from the critical load with the arrester, P_C , and the FEM model for arrester-free specimen of the same crack length, a , to indicate the arrester effect. Under all types of loading, the fracture toughness of arrester-free specimen, G_C , is constant independent of crack length, and the $G_C(\text{apparent})$ of the arrester specimen significantly increases with decreasing distance from the crack tip to the edge of the arrester. Under mode I type loading, the apparent fracture toughness of the arrester specimen increased 1.3-fold at the point of the initial crack ($a = 50$ mm) and by 5.1-fold in the vicinity of the arrester edge ($a = 67$ mm) [6]. Under mixed-mode type loading, $G_C(\text{apparent})$ increased 1.6-fold at the position of the initial crack ($a = 50$ mm) and 6.7-fold in the vicinity of the arrester edge ($a = 62$ mm). Under mode II type loading, $G_C(\text{apparent})$ increased 1.2-fold at the point of the initial crack ($a = 50$ mm) and 2.0-fold in the vicinity of the arrester edge ($a = 69$ mm) [7]. If the crack did not kink near the edge of the arrester, the $G_C(\text{apparent})$ might have been much higher. The suppression effect of the crack arrester was confirmed from these results.

Fig.11 shows G_C values and crack lengths under mode I type [6], mixed-mode type, and mode II type [7] loadings fracture toughness tests. Here, the G_C values for the arrester specimen were net values, and obtained from the critical load using the FEM model with the arrester. Under mode I and mixed-mode type loadings, the G_C values of the arrester specimen were higher than those of the arrester-free specimen. The net G_C values of the arrester and arrester-free specimens should be the same.

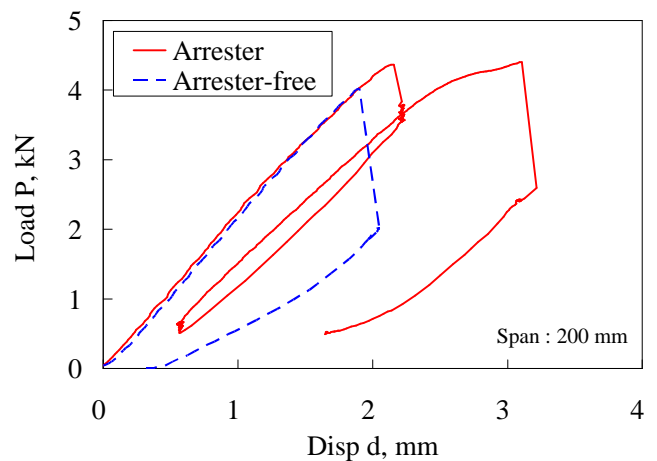
The differences in net G_C may be caused by differences in residual stress or the thickness of the resin layer [9] between the arrester and arrester-free specimens. Further research is necessary.



a) Mode I type loading

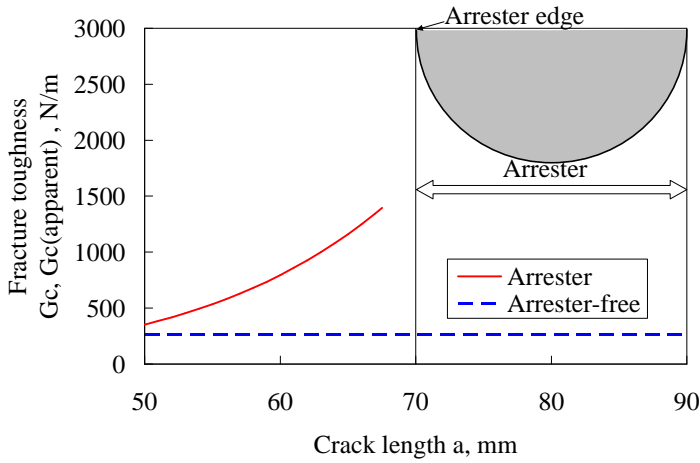


b) Mixed-mode type loading

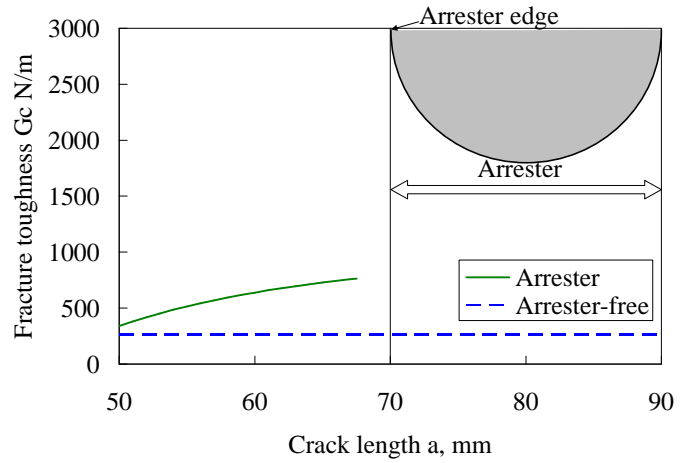


c) Mode II type loading

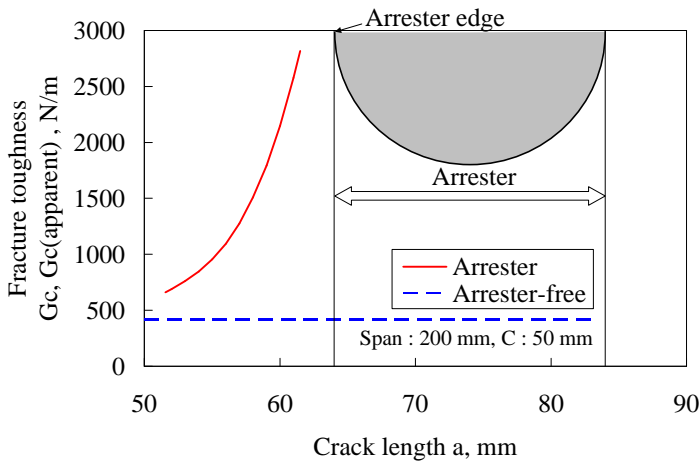
Fig.9 Relationship between applied load and displacement



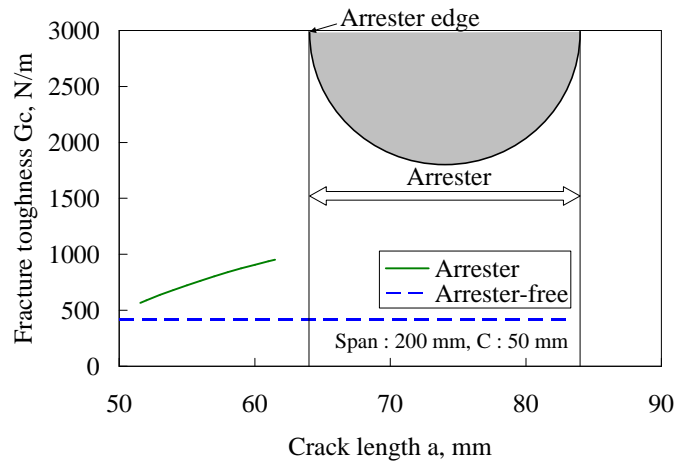
a) Mode I type loading



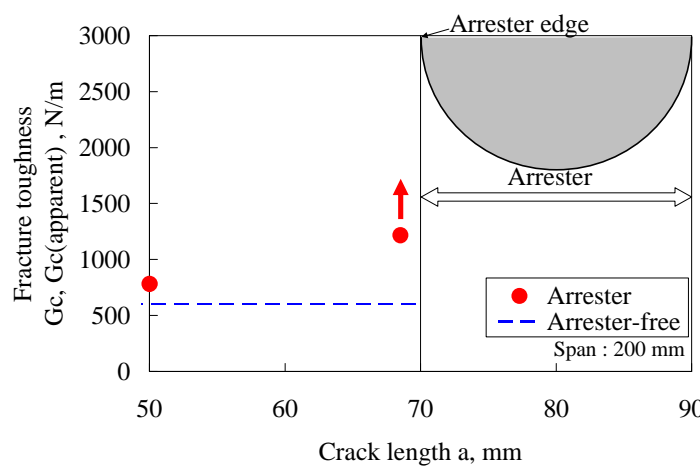
a) Mode I type loading



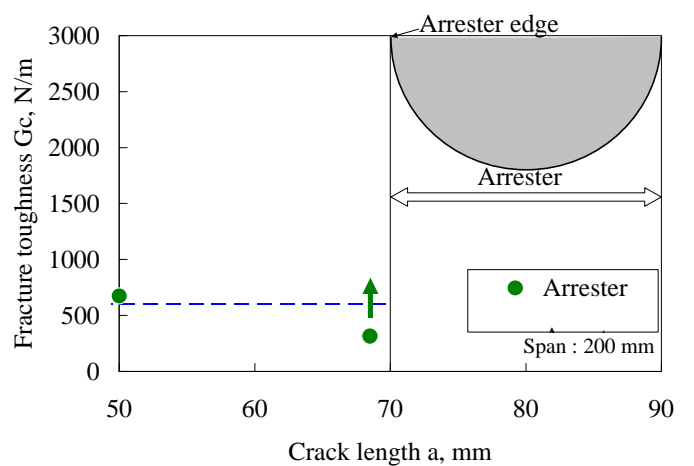
b) Mixed mode type loading



b) Mixed mode type loading



c) Mode II type loading



c) Mode II type loading

Fig.10 Relationship between apparent fracture toughness and crack length

Fig.11 Relation between net fracture toughness values and crack length

5 Influence of loading type

Fig.12 shows the G_C values of the arrester-free specimens under mode I, mixed-mode, and mode II type loadings. The G_C depends on loading type, and increases with increasing contribution of mode II type loading, as observed in the delamination of GFRP [10].

Fig.13 and Table 2 show a comparison of the apparent and net G_C values of the arrester specimen, and those of the arrester-free specimen. The difference in the net value between the arrester-free and the arrester specimens is constant regardless of loading type. The total suppression effect of the arrester, $G_C(\text{apparent})/G_0$, is 5.1-fold under mode I type, 6.7-fold under mixed-mode type, and over 1.9-fold under mode II type loadings. If the crack did not kink near the edge of the arrester, $G_C(\text{apparent})$ might be higher. The structural suppression effect of the arrester, $G_C(\text{apparent})/G_C(\text{net})$, is 2.0-fold under mode I type, 3.2-fold under mixed-mode, and over 3.9-fold under mode II type loadings. The structural effect under mode II type loading is the highest, and this attenuates with increasing contribution of the mode I type component. This tendency agrees with the analytical result.

The design criterion for the mixed-mode loading is necessary because various types of load are expected for civil aircraft applications. On the other hand, crack propagation at the interface between the resin layer and the core is an interfacial crack issue. Loading type is different from the mode ratio of the crack tip based on complex stress intensity factors. Therefore, a design criterion under the mixed-mode loading is necessary to separate the influence of each mode on the crack tip. The design chart should be developed considering the correlation of the mode ratio of the crack tip and the loading mode ratio of civil aircraft members.

6 Conclusions

It was found by the numerical simulation that G decreases as the crack tip approaches the arrester edge. The suppression effect of the crack arrester was confirmed by fracture toughness test. The suppression effect of the arrester under mode II type loading is the highest, which attenuates with increasing contribution of the mode I type component. This tendency agrees with the analytical result.

This study was sponsored by the Society of Japanese Aerospace Companies.

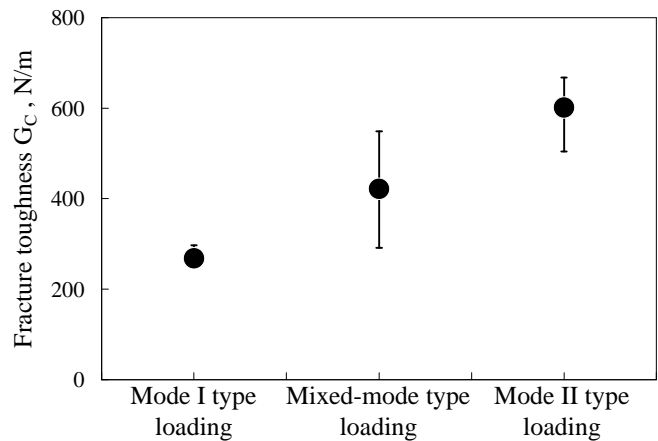


Fig.12 Relationship between net fracture toughness and loading type.

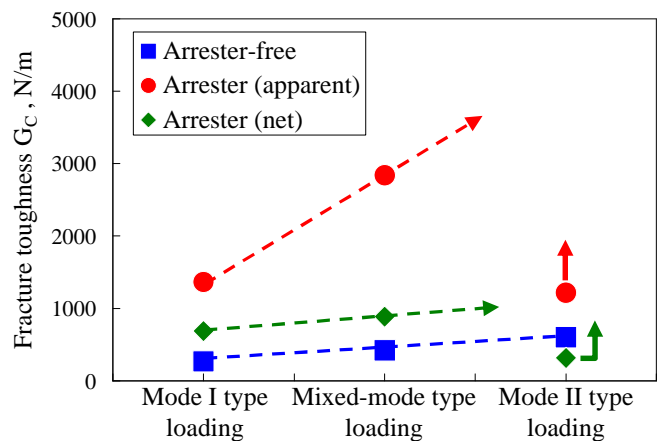


Fig.13 Relationship between apparent fracture toughness and loading type.

Table 2 Arrester effect evaluated from fracture toughness.

	Mode I type loading	Mixed-mode type loading	Mode II type loading
$G_C(\text{apparent}) / G_{C0}$	5.1	6.7	Over 2.0
$G_C(\text{apparent}) / G_C(\text{net})$	2.0	3.2	Over 3.9

References

- [1] S. Ochi, Y. Hirose, M. Nishitani, T. Sana, T. Ito, Y. Ikeda, H. Kikukawa, "Development of CFRP sandwich panel structure for transport nose component", Proc The 9th European-Japanese Symposium on Composite Materials, Hamburg, Germany, 2004
- [2] Y. Ikeda, Y. Hirose, M. Nishitani, S. Ochi, T. Ito, "Development of foam core sandwich panel structure for transport nose structure", Proc. 5th Gyeongnam (Korea)-Tokai (Japan) Aerospace Technology Symposium, Sacheon, Korea, pp.67-78, 2004.

- [3] L. Herbec, "Technology and design development for a CFRP fuselage", Presented at 25th SAMPE Europe Conference, Paris, France, 2003
- [4] Y. Hirose, M. Hojo, A. Fujiyoshi, G. Matsubara, "Suppression of interfacial crack for foam core sandwich panel with crack arrester" *Advance Composite Material*, in press.
- [5] Y. Hirose, M. Hojo, A. Fujiyoshi, G. Matsubara, "Suppression of interfacial crack for foam core sandwich panel with crack arrester" *Proc. 9th Japan International SAMPE Symposium & Exhibition*, 2005.
- [6] Y. Hirose, G. Matsubara, M. Hojo, H. Matsuda, F. Inamura, "Evaluation of mode I crack suppression method for foam core sandwich panel with fracture toughness test and analyses", *Proc. Composite Material Congress 2006, Japan*, pp.83-84, 2006
- [7] Y. Hirose, G. Matsubara, M. Hojo, H. Matsuda, F. Inamura, "Evaluation of mode II crack suppression method for foam core sandwich panel with fracture toughness test and analyses", *Proc. Mechanical Engineering Congress 2006, Japan*, vol.6, pp.171-172, 2006.
- [8] E. F. Ryubicki, M. F. Kanninen, "A Finite element calculation of stress intensity factors by a modified crack closure integral", *Eng. Frac. Mech.*, 9, pp.931-938, 1977.
- [9] M Hojo, T Ando, M Tanaka, T Adachi, S Ochiai, Y Endo, "Mode I and II interlaminar fracture toughness and fatigue delamination of CF/epoxy kaminates with self-same epoxy interleaf", *Int. J. Fatigue* 28,pp.1154-1165, 2006.
- [10] G Matsubara, H Nishikawa, K Nihei, K Tanaka, "Mode-mixity effect on growth behavior of interlaminar fatigue cracks in high strength GFRP", *Trans. Jpn. Soc. Mech. Eng.*, (in Japanese), vol.70, No.700, A(2004), pp.1733-1740.